# Title: Emergent climate change patterns originating from deep ocean warming in climate mitigation scenarios

**Author list: Ji-Hoon Oh[1], Jong-Seong Kug*[1,2], Soon-Il An[1,3], Fei-Fei Jin[4], Michael McPhaden[5], and Jongsoo Shin[6]**

**Affiliations:** [1]Division of Environmental Science and Engineering, Pohang University of Science and Technology (POSTECH), Pohang, South Korea.

[2]Institute for Convergence Research and Education in Advanced Technology, Yonsei University, Seoul, South Korea.

[3]Department of Atmospheric Sciences / Irreversible Climate Change Research Center, Yonsei University, Seoul, South Korea.

[4]Department of Atmospheric Sciences, University of Hawaii, Honolulu, USA.

[5]NOAA / Pacific Marine Environmental Laboratory, Seattle, USA.

[6]Wodds Hole Oceanographic Institution, Woods Hole, Massachusetts, USA.

[*]Corresponding author: Jong-Seong Kug (email: jskug1@gamil.com)

Prof. Jong-Seong Kug, Division of Environment Science and Engineering, Pohang University of Science and Technology, Pohang 37673, South Korea

**Abstract**

The global oceans absorb most of the surplus heat from anthropogenic warming, but it is unclear how this heat accumulation will affect the Earth's climate under climate mitigation scenarios. Here, we show that this stored heat will be released at a much a slower rate than its accumulation, resulting in a robust pattern of surface ocean warming and consequent regional precipitation. The surface ocean warming is pronounced over subpolar-to-polar regions and the equatorial eastern Pacific where oceans are weakly stratified to allow vigorous heat release deep ocean to the surface layer. It is also demonstrated that this ocean warming pattern largely explains changes in the precipitation pattern including southward shift of the Intertropical Convergence zone and more moistening in high latitudes. This study suggests that deep ocean warming may hinder climate recovery in some regions, even if carbon neutrality or net negative emissions are successfully achieved.

## Main text

The ocean, covering more than 70% of Earth's surface, exerts a critical role in regulating the climate system. It has absorbed more than 90% of the current energy imbalance (surplus heat) caused by persistent emissions of anthropogenic greenhouse gases (GHGs), particularly carbon dioxide ($CO_2$)[3–5]; thus, the ocean plays a role in slowing down global surface warming. Indeed, a global warming hiatus from 2002 to 2012[6] was associated with enhanced subsurface ocean heat uptake in the equatorial Pacific[7,8]. Widespread and significant ocean warming has been observed since the 1950s and it continues to accelerate[9,10].

A key characteristic of ocean warming is the various response timescales of different ocean depths to climate forcings. The ocean mixed layer responds rapidly to surface heating due to direct interaction with the atmosphere, while the deeper ocean adjusts much more slowly due to its larger thermal inertia and slow heat transport into it[11]. As a result, deep ocean warming is expected to persist for centuries even after achieving net-zero $CO_2$ emissions[12,13]. In other words, today's greenhouse gas emissions will have enduring impacts on future ocean changes, giving a long-term memory to our climate system in response to anthropogenic forcing.

Under the potential threats from anthropogenic climate change, a worldwide commitment has been pledged to limit global warming to below 2°C, and preferably to 1.5°C, as codified in the 2015 Paris Agreement. This goal requires immediate and decisive international action to achieve net zero and negative $CO_2$ emissions[14–17], not only by reducing anthropogenic $CO_2$ emissions, but also by artificial techniques to remove $CO_2$ from the atmosphere. This crucial step is essential to restore the climate system and ensure a sustainable future. Accordingly, recent studies have investigated the hysteresis and reversibility of global or regional climate in response to atmospheric $CO_2$ removal by using idealized climate model experiments[2,18–34]. Global total ocean heat content (OHC) and the resultant thermosteric sea level rise associated with the slow response of the deep ocean have exhibited the clearest irreversible response across the different climate models despite the rapid $CO_2$ removal (e.g., 1% year$^{-1}$ or even 5% year$^{-1}$) to the present level[22–24]. To avoid ambiguity, the term "irreversible change" here is used as a long-term transient recovery on a multi-century timescale (more than 200yrs) that is humanly perceptible after the $CO_2$ concentration returns to baseline.

Such an irreversible response of ocean warming as a result of past anthropogenic GHGs emissions may modulate global or regional surface climate[11,35–38] in addition to changes in sea level and the marine environment itself. From a global perspective, the sole way to diminish the heat absorbed by the ocean from the atmosphere is to release it back into the atmosphere. For example, the deeper ocean may gradually transport stored heat to the upper ocean and mixed layers, ultimately being released back into the atmosphere. This potential long-term counteractive effect of the ocean as a heat source for the surface climate system can persist over centuries. Hence, there is a possibility that the ocean's thermal inertia may affect the surface climate system in terms of both timescale and regional pattern. Analyzing this aspect can provide vital information for regional climate adaptation and mitigation strategies from a long-term perspective. Despite this importance in the long-term perspective, an active role of the deep ocean as a heat source for the surface climate has often been overlooked, mainly due to its predominant recognition as a thermal buffer. This perspective stems from the dominance of radiative forcing caused by the rapid increases in GHGs. However, the counteractive effect of the ocean will be clearer under a net negative $CO_2$ emission scenario, owing to the discrepancy of adjustment timescale between the surface and deep ocean in response to $CO_2$ removal.

Here, the active role of deep ocean warming on the surface climate is mainly explored. To address this scientific question, a large ensemble experiment is performed by employing the Community Earth System Model (CESM) with 28 ensemble members. In this experiment, the atmospheric $CO_2$ concentration increases by 1% per year for 140 years until it quadruples (Ramp-up), then declines symmetrically to the initial $CO_2$ level (Ramp-down) and is held constant for 220 years thereafter (Restoring, see Methods for details).

**Irreversible response of deep ocean warming**

In response to $CO_2$ forcing, the global total (globally and full-depth integrated) OHC clearly exhibits an irreversible change (Fig. 1a,b). After about 85 years (year 2235) from the $CO_2$ peak, the global total OHC anomaly reaches the maximum (~ $4.3\times10^{24}$ J), which corresponds to ~ 60 cm rise in global thermosteric sea level. It then begins to decrease slowly but still represents ~ 62% of the maximum at the end of the simulation even after about 200 years since the $CO_2$ level has returned to the present climate level, indicating an irreversible change on a human timescale. This suggests that even if the initial $CO_2$ level is fully restored, the fingerprint of past global warming remains in the global ocean in the form of massive heat. Indeed, the temporal evolution of the total OHC is almost identical to the accumulated surface heat flux from the atmosphere, confirming a heat balance between the ocean and the atmosphere (Fig. 1a).

The irreversible response of ocean warming is associated with the slow response of the deep ocean[11,12,24,36]. Here, the below 700m oceans is defined as the "deep ocean" based on the climatological global pycnocline depth, which is roughly found around 700m[39,40] (varying from 500 to 1000m) and much of modern ocean warming is observed in the upper 700m [10]. Indeed, the temperature response to radiative forcing is more delayed with depth (Fig. 1b). The ocean temperature in the upper 700m begins to decrease during the ramp-down period, while the temperature between 700m and 2000m continues to increase until the onset of the restoring period, so that, at this time, the maximum temperature anomaly occurs at about 700m. However, water below 2000m exhibits a slow and sustained increase in temperature since this layer is still adjusting to the past increased atmospheric $CO_2$ concentration. Thus, the overall temporal evolution of total OHC is largely explained by

OHC above 2000m (Fig. 1b). Additionally, to examine the spatial pattern of irreversible OHC response, the total OHC distribution (Fig. 1c) is averaged over the last 100 years of the simulation (light blue box in Fig. 1a). It exhibits overall positive signals across the globe but is especially pronounced in the Atlantic and the Southern Ocean due to previous active local ocean heat uptake (OHU, downward net surface heat flux) and its redistribution by the meridional overturning circulation[10,41–44] (Fig. 1c).

An important feature is that the global total OHC begins to slowly decrease in accordance with rapid reduction and subsequent stabilization of atmospheric $CO_2$ concentration, even if there is a delay of decades after the $CO_2$ peak (Fig. 1a). This loss of total OHC is primarily attributed to the loss in the upper 2000m (Fig. 1b). Since the sign of global OHU changes from positive to negative around year 2235 (maximum of global total OHC), the global total OHC begins to decrease. This corresponds to a net heat loss to the atmosphere across the sea surface, which implies a net transition in the role of the ocean from a heat sink to a heat source for the atmosphere. This may hinder the recovery of surface climate by continuous heat supply, which eventually can contribute to the hysteresis and irreversibility of global or regional climate.

**Spatial patterns of the irreversible surface climate changes**

To explore the ocean warming-induced irreversible pattern of surface climate, here the irreversible change and its pattern are defined as the difference between the time average of the last 100 years (years 2401−2500) of the simulation and the 900yrs mean of the present-day control simulation (see Methods). The irreversible pattern of sea surface temperature (SST) shows overall positive signals, indicating that the SST remains higher than in the present climate. Notably, SST pattern exhibits distinct delayed responses over the subpolar regions such as the Southern Ocean (SO), subpolar North Atlantic (SPNA), and Bering Sea (BS). An El Niño-like pattern is also evident in the equatorial eastern Pacific (EEP) (Fig. 2a). This spatial pattern is similar to the slow response to global warming reported in the previous literatures[11,35,37,45] which is partially obscured by the fast-varying surface warming pattern. The long-lasting and specific SST pattern is hypothesized to be associated with irreversible ocean warming, leading to the natural inquiry of understanding their dynamic connection.

Next, the patterns of total OHC and SST over the last 100 years of the simulation are compared to examine the linkage between them. It is evident that the SST pattern (Fig. 2a) does not correspond to that of total OHC (Fig. 1c), indicating that the local OHC response does not directly link to local SST. That is, even if a larger heat remains in a water column, it is not directly connected to higher SST. A plausible explanation for the irreversible SST pattern could be related to spatial distribution in the background ocean stratification. This distribution can roughly indicate how effectively properties and tracers such as carbon and heat in the deeper ocean are ventilated into the upper ocean. Indeed, recent studies have reported that the climatological ocean circulation and stratification are strongly related to the future heat and carbon uptake[46] and the distribution of their storage[47].

It is hypothesized that background ocean stratification might be a key factor for the linkage between the irreversible patterns of OHC and SST. Ocean stratification is roughly represented by the squared buoyancy frequency ($N^2$) averaged over the upper 2000m (Fig. 2b) where OHC loss occurs (Fig. 1b). The $N^2$ is positive because the density increases with depth. Oceans with a smaller $N^2$ exhibit lower static stability, characterized by relatively stronger residual upwelling of dense deep water or vertical mixing that occurs both along and across isopycnals. These processes weaken vertical density gradient in the water column. Therefore, it is possible that in oceans with smaller $N^2$, the accumulated heat in deeper depths can be more efficiently ventilated. Indeed, the spatial pattern of the background $N^2$ shows some similarity to the irreversible SST pattern (Figs. 2a,c), although the detailed regional patterns are different. In particular, weakly stratified background conditions are found in areas of apparent SST irreversibility, such as SO, SPNA, BS, and EEP.

More specifically, vigorous wind-driven upwelling, as measured by Eulerian vertical velocity ($W_{eulerian}$) in the subpolar gyre and equatorial ocean is observed as well as south of the Antarctic Circumpolar Current (ACC) including SO, SPNA, BS, and EEP (Extended Data Fig. 1). These intense upward motions extend coherently to depths at least 1000m, and are partially offset by mesoscale eddy-induced vertical velocity ($W_{eddy-induced}$, i.e., bolus velocity) parameterized following Gent and McWilliams (1990)[48] (Extended Data Fig. 2). Consequently, the resulting residual upwelling ($W_{residual} = W_{eulerian} + W_{eddy-induced}$) can effectively transport heat from the deeper layer to the mixed layer along the sloped isopycnals (Fig. 2c). In regions where the winter mixed layer is deep, the heat can be effectively supplied into the surface. Notably, in the Labrador Sea, located in the SPNA, there is a particularly strong process for efficiently mixing up the heat deposited at depths up to ~2000m (light pink and blue shadings in Fig. 2c and Extended Data Fig. 3a). The enhanced meridional oceanic heat transport due to the overshoot of the Atlantic Meridional Overturning Circulation (AMOC, Extended Data Fig. 4)[18,48], also plays a role in the distinct SST irreversibility in the SPNA. Furthermore, the mesoscale eddy-induced mixing along the tilted isopycnals, which is parameterized by the diffusion operator with isopycnal diffusivity following Redi (1982)[49] (Extended Data Fig. 3b), contributes to the heat exchanges between the deeper and surface layers.

In summary, the heat accumulated in the deep ocean by global warming is effectively ventilated in specific regions through the vigorous residual upwelling and isopycnal and diapycnal mixing processes, facilitating active heat exchanges there and ultimately delaying SST recovery. In addition, once the heat is released to the surface, strong positive feedbacks[50] such as sea-ice albedo and low cloud-SST feedback[51,52] (Extended Data Fig. 5) further amplify the warming by increasing downward solar radiation over the subpolar to polar areas and along the west coast of the continent (e.g. sea-ice and low cloud reduction patterns in Extended Data Fig. 5). This complex interplay of both oceanic upward heat transfer and atmospheric positive feedbacks eventually shapes the detailed long-lasting SST pattern as a result of irreversible ocean warming. Considerable deep ocean warming is prevalent over the whole global ocean even in the end of the simulation. Hence, the irreversible SST pattern is largely explained by local ocean ventilation in the background state regardless of the horizontal distribution of OHC anomaly.

Additionally, such an SST pattern plays a role in shaping the irreversible pattern of the hydrological cycle. Due to the higher SST than the present climate across the globe (Fig. 2a), precipitation responses are also overall enhanced (Fig. 2d). For example, there are distinct precipitation increases over the SO and SPNA, consistent with the regions where the SST increases are the strongest. The most pronounced feature of the precipitation response is the southward shift of the intertropical convergence zone (ITCZ) in the Pacific and Atlantic Oceans, characterized by a rainfall decrease along the climatological ITCZ and an increase south of that. This feature is also closely related to the SST pattern. According to the energetic framework, the latitudinal position of ITCZ is associated with cross-equatorial energy transport regulated by meridional energy exchanges between hemispheres[53–56]. Therefore, widespread warming in the SO can pull the ITCZ to the south by weakening the poleward atmospheric energy transport from the tropics to extratropics in the Southern Hemisphere[28]. Moreover, the El Niño-like SST pattern also leads to a local ITCZ shift to the south[57], which further enhances the precipitation response in the EEP; this tropical rainfall variation may affect the formation of the extratropical rainfall pattern via atmospheric teleconnections[58]. On the basis of this dynamical relationship between the SST and precipitation patterns, it is highlighted here that the horizontal distribution of the background ocean stratification is also important for shaping the irreversible pattern of the hydrological cycle as well as that of temperature. Additionally, CMIP6 models and the inter-ensemble relationship further support our argument (Extended Data Fig. 6-8 and supplementary Figs. 1-3).

**Evidence from initial warming experiments**

So far, it is suggested that the irreversible SST pattern is determined by the slow ocean warming and climatological distribution of the ocean stratification. However, the surface climate changes are highly complex in the coupled climate system since they are influenced by various factors and feedbacks (such as sea-ice albedo or low cloud-SST feedback, Extended Data Fig. 5) in addition to the vertical heat exchanges. Therefore, it should be careful to conclude solely from statistical analysis and spatial similarity that the irreversible patterns of surface temperature and hydrological cycles indeed originate from deep ocean warming.

To supplement our arguments, four additional initial warming experiments (named IW_whole, IW_be100, IW_be700, and IW_ab100) are conducted to explore the intrinsic role of stored heat in the deep ocean in shaping a particular surface climate pattern. All initial warming experiments are integrated with constant atmospheric $CO_2$ concentration, but spatially uniform temperature and salinity perturbation profiles were added to the ocean's initial condition (see Methods). That is, the initial temperature and salinity perturbations are entirely identical across all ocean grids. The added initial perturbations are the vertical profile of the global mean temperature and salinity at the year 2280 when the $CO_2$ concentration first returned to the year 2000 level (Fig. 3a). Specifically, to isolate the effect of the deep ocean, the initial warming is added to the whole depth, below 100m depth, below 700m depth, and upper 100m depth in the IW_whole, IW_be100, IW_be700, and IW_ab100, respectively. By investigating how this uniform initial warming emerges to the surface, it is found that the background local ocean stratification is an important factor in the irreversible SST pattern as a bridge between the deep ocean and the surface.

When the initial warming is given in the upper 100m (IW_ab100), the immediate global mean SST (GMST) increase rapidly decays due to the intense heat release into the atmosphere. However, in the presence of deep ocean warming, the GMST gradually increases up to about 1.2K (IW_whole and IW_be100) and 0.6K (IW_be700) (Fig. 3b), and then slowly decays. This implies that the cumulative heat in the deep ocean is still capable of considerably raising GMST, even though atmospheric $CO_2$ concentrations have totally returned to the present level. This slow process can induce irreversible behavior in the surface climate system. Compared to the IW_whole and IW_be100, the GMST in the IW_be700 slowly evolves and it becomes close to that of IW_whole during the last 50 years despite the smaller total heat of initial thermal perturbation than that of the IW_whole. It is worthwhile noting that GMST in the three IW_EXPs with deep ocean warming gradually decreases but it is still not totally back to the initial level for at least 150 years.

More importantly, it is found that the three experiments (IW_whole, IW_be100, and IW_be700) reveal quite similar SST and precipitation patterns in the last 50 years, suggesting that uniform deep ocean warming prefers a particular horizontal pattern of the surface climate. Strikingly, the spatial patterns of both SST and precipitation in the three IW_EXPs are highly similar to those of the irreversible patterns shown in Fig. 2, with significant spatial correlation coefficients of 0.94, 0.95, 0.92 (SST), and 0.91, 0.92, 0.90 (precipitation) in the IW_whole, IW_be100, and the IW_be700, respectively (Fig. 3c-d and Extended Data Fig. 9). In addition to the SST pattern, a high spatial resemblance is also observed in the land surface temperature (Extended Data Fig. 10). This spatial similarity despite a uniform deep ocean warming clearly demonstrates that the combination of deep ocean warming with the local distribution of the background stratification shaped by the vertical upwelling and mixing is a key factor in shaping the irreversible surface climate changes.

One may argue that the irreversible SST pattern could be mainly shaped by the strong positive feedbacks in the subpolar-to-polar areas, not by local ocean stratification. However, when the initial warming is only added to the surface layer (~100m, IW_ab100), the spatial patterns of SST, precipitation, and land surface temperature exhibit no consistency with the patterns in Fig. 2 (Extended Data Fig. 9e-f and Fig. 10e). These results imply that although various factors contribute to the shape of surface climate, such as air-sea interaction, the fundamental cause of the irreversible pattern of surface climate originates from the release of deep ocean heat where vertical heat exchange is relatively vigorous.

## Discussion

It has been well documented that the ocean plays a role in slowing down global surface warming by absorbing most of the Earth's radiative imbalance due to anthropogenic GHGs. However, it is demonstrated here that the accumulated heat in the deep ocean will bring about irreversible climate change by eventually releasing the heat into the atmosphere[11,34–36,38]. In particular, the deep ocean warming-induced irreversible climate change stands for a specific spatial pattern, which is closely related to climatological ocean stratification. Heat release from the deep ocean to the surface depends largely on the extent of the global ocean stratification, thus it naturally takes a long time for heat to be transported to the surface given the strong background ocean stratification. In addition to this background stratification in the global ocean, positive local feedbacks exerts a role in slowing the heat release from the deeper depth over the weakly stratified oceans. For example, the deep ocean-induced surface warming simultaneously accompanies the local positive feedbacks[50] such as the sea ice-albedo and low cloud-SST feedbacks[52,59] (Extended Data Fig. 5), which can amplify or maintain the positive SST perturbation by minimizing outgoing surface heat flux toward the atmosphere. In other words, the heat loss into the atmosphere occurs inefficiently despite the considerable surface warming, thus the OHC loss evolves slowly, resulting in strong irreversible ocean warming (Fig. 1) and further irreversible surface climate changes (Fig. 2). A quantitative analysis of the role of these surface feedbacks in diminishing surface heat loss, and thereby strengthening the irreversibility of SST and deep ocean heat loss should be addressed in a further study.

Even though this study focused on the irreversible response in the restoring period after the ramp-down scenario, the effect of deep ocean warming on the surface climate would always operate when considerable deep ocean warming exists. For example, even when we successfully achieve net zero emissions, the deep ocean warming-induced climate patterns would emerge and impact the global climate. Therefore, how much and/or how long the GHGs will be emitted until reaching net zero emissions determine the amount of accumulated warming in the deep ocean, which will be a critical factor in determining the recovery of Earth's climate. On the contrary, when the atmospheric $CO_2$ concentration is changing, whether increasing or decreasing, the effect of the deep ocean warming can be hidden in the patterns of fast responses to strong radiative forcing and associated complex feedbacks. However, the deep ocean warming definitely plays a role in our climate system and its impacts will be stronger and sustained longer if the accumulated deep ocean warming is larger. Therefore, we still need to take the effect of the deep ocean-induced climate pattern into account for long-term climate projections.

**Acknowledgments**

The CESM simulation and data transfer were supported by the National Supercomputing Center with supercomputing resources (KSC-2023-CHA-0001), the National Center for Meteorological Supercomputer of the Korea Meteorological Administration (KMA), and the Korea Research Environment Open NETwork (KREONET), respectively. J.-S. Kug was supported by the National Research Foundation of Korea (NRF) grant funded by the Korean government (NRF-2022R1A3B1077622). S.-I. An was supported by the National Research Foundation of Korea (NRF-2018R1A5A1024958). This is PMEL contribution no. 5451

**Author Contributions Statement**

J.-H. Oh compiled the data, conducted analyses and simulations, prepared the figures, and wrote the manuscript. J.-S. Kug designed the research and wrote the manuscript. All authors discussed the results and revised the manuscript.

**Competing Interests Statement**

The authors declare no competing interests.

## Figure Legends / Captions

**Fig. 1 | Temporal evolution and spatial pattern of the ocean warming. a**, Temporal evolution of applied $CO_2$ concentration forcing (black), ensemble mean of the global total (globally and full-depth integrated) ocean heat content (OHC, blue), ocean heat uptake (OHU, i.e. net surface heat flux, red) and cumulative (time-integrated) OHU (dotted red). Lines and light shadings indicate 28 ensemble means and full ensemble spread, respectively. The light red and blue boxes in panel **a** indicate the year 2235 (OHC peak phase) and the last 100 years of the simulation. **b,** Temporal evolution of the vertical profile of the global mean ocean temperature every 20 years. The red, blue, and gray line colors represent the ramp-up, -down, and restoring periods, respectively. The insert plot in panel **b** shows the temporal evolution of the globally and vertically integrated ensemble mean OHC. The light red, red, and dark red colors represent the 0−700m, 700−2000m, and below 2000m integration, respectively. All time series are based on annual means relative to year 2000 and smoothed by an 11-year running mean. **c**, Total OHC anomaly averaged over the last 100 years (year 2401−2500) relative to year 2000. Only values significant at the 95% confidence level are shown in panel **c**.

**Fig. 2 | Spatial patterns of the irreversible surface climate changes. a, d,** As in Fig. 1**c**, but for the sea surface temperature (SST) and precipitation. The black contour line in panel **d** denotes the background annual ocean precipitation of 5 mm day$^{-1}$ within 30°S–30°N. **b,** Background upper 2000m averaged squared buoyancy frequency ($N^2$). The black contour line in panel **b** is the background $N^2$ of $0.15 \times 10^{-4}$ s$^{-2}$. Note that the order of the colors in panel **b** is in reverse. **c,** Background residual (sum of eulerian and bolus vertical velocities) ocean vertical velocity ($W_{residual}$) at 700m. Only upwelling regions are displayed to highlight the result. The light pink and blue shadings denote areas where the maximum background mixed layer depth (monthly maximum among 12 months climatology in each grid) exceeds 150m and 700m, respectively. Here, the "background" (overbar) refers the long-term mean of each physical quantity in the present-day control simulation (year 2000 level).

**Fig. 3 | Design and results of the initial warming experiment. a,** Global mean potential temperature (red) and salinity (black) profile at the year 2280 when the $CO_2$ concentration first returned to the present level. These two vertical profiles are uniformly added to all ocean grids of the model's original initial condition (year 2000 condition). The two gray horizontal lines denote the 100m and 700m depth, respectively. The red, blue, yellow, and black vertical bars indicate the depth of the initial forcing used in each experiment (see Methods for a detailed description of the initial warming experiment). **b,** Temporal evolution of ensemble mean of the global mean SST of IW_whole (red), IW_be100 (blue), IW_be700 (green), and IW_ab100 (black) relative to the year 2000. The light and solid lines denote yearly evolutions and evolutions after being smoothed by a 5-year running mean, respectively. **c, d,** SST, and precipitation anomalies averaged over the last 50 years (2101−2150) of IW_whole relative to year 2000. The black contour line in panel **d** denotes the climatological annual mean ocean precipitation of 5 mm day$^{-1}$ within 30°S–30°N. Only significant values at the 95% confidence level are shown in panels **c** and **d**. The numbers labeled at the upper top corner in panels **c** and **d** are the pattern correlations between each panel's pattern and the reference irreversible SST and PRCP patterns (Fig. 2a and 2d).

## Methods

### Dataset and experimental design

This study employed the Community Earth System Model, Version 1.2 (CESM1.2) which incorporates the Community Atmospheric Model Version 5 (CAM5), Community Land Model Version 4 (CLM4), the Community Ice Code Version 4 (CICE4), and the Parallel Ocean Version 2 (POP2). The CAM5 and CLM4 used a horizontal resolution of ~1°, with 30 vertical levels. The CICE4 and POP2 used a nominal 1° horizontal resolution (the meridional resolution was ~1/3° near the equator), with 60 vertical ocean levels.

Two kinds of idealized climate model simulations were conducted. One was a present-day simulation with a constant atmospheric $CO_2$ concentration (present-day level, 367 ppm) integrated over 900 years. The second was a $CO_2$ ramp-up and ramp-down simulation and branched from the different 28 initial conditions in the present-day simulation. This experiment increased the atmospheric $CO_2$ concentration at a rate of 1% year$^{-1}$ until it was quadrupled (1468 ppm) over 140 years, then symmetrically decreased $CO_2$ concentration at the same rate for 140 years until it reached the initial value (367 ppm). Subsequently, a restoring experiment is conducted with a constant $CO_2$ concentration (367 ppm) for 220 years, representing a net-zero emissions period. The total period for the second experiment was 500 years, and it included 28 ensemble members. This experimental design is the same as that used by the 1pct$CO_2$-cdr scenario from the Carbon Dioxide Removal Model Intercomparison Project (CDRMIP)[60], except for the initial $CO_2$ level (pre-industrial level, 284.7 ppm).

It is also used historical, 1pct$CO_2$ and 1pct$CO_2$-cdr scenarios based on 8 CMIP6 models: ACCESS-ESM1-5, CESM2, CNRM-ESM2-1, CanESM5, GFDL-ESM4, MIROC-ES2L, NorESM2-LM and UKESM1-0-LL. Each model of 1pct$CO_2$-cdr scenario has a different length of restoring period prescribing constant $CO_2$ forcing: 620 years, 60 years, 60 years, 160 years, 60 years, 362 years, 119 years, and 510 years. The CMIP6 dataset was used after re-griding to 1° × 1° horizontal resolution.

**Design of the initial warming experiment**

To explore the role of deep ocean warming in shaping the irreversible SST pattern, four kinds of initial warming experiments (named IW_whole, IW_be100, IW_be700, and IW_ab100) are carried out. All IW_EXPs were branched from the initial condition (year 2000) of each ensemble member and integrated with constant atmospheric $CO_2$ concentration (367 ppm), except that the horizontally uniform temperature anomaly profile was added to the initial ocean condition. The added temperature anomaly was the global mean potential temperature at the year 2280 when the $CO_2$ concentration first returned to its initial value (Fig. 3a). To prevent a potential imbalance of density, the salinity anomaly profile is also added to the initial ocean condition. That is, in all grids, the initial temperature and salinity perturbations are identical. Note that the initial warming was applied to the whole depth, below 100m, below 700m, and upper 100m in IW_whole, IW_be100, IW_be700, and IW_ab100, respectively, in order to isolate the deep ocean's intrinsic role. All IW_EXPs were integrated for 150 years with 9 ensemble members, except that the IW_ab100 had 3 ensemble members.

**Stratification metric**

In this study, the ocean stratification (static stability) is measured as the squared buoyancy frequency ($N^2$):

$$N^2 = -g \frac{1}{\rho_0} \frac{\partial \rho}{\partial z} \quad (1)$$

, where g, $\rho_0$, and $\rho$ is the seawater density, gravitational acceleration, and potential density, respectively.

**Data Availability**

The data used in this study are available from https://doi.org/10.6084/m9.figshare.24873216.v1 (ref. 61), and the CMIP6 archives are freely available from https://esgf-node.llnl. gov/projects/cmip6.

**Code availability**

The codes used in this study are available from https://doi.org/10.6084/m9.figshare.24873216.v1 (ref. 61). All figures were generated by using software package Python with the matplotlib and basemap modules (https://matplotlib. org/, https://matplotlib.org/basemap/).

## Reference


1. Meyssignac, B. *et al.* Measuring Global Ocean Heat Content to Estimate the Earth Energy Imbalance. *Front Mar Sci* **6**, (2019).
2. von Schuckmann, K. *et al.* Heat stored in the Earth system: where does the energy go? *Earth Syst Sci Data* **12**, 2013–2041 (2020).
3. Cheng, L. *et al.* Improved estimates of ocean heat content from 1960 to 2015. *Sci Adv* **3**, (2017).
4. Easterling, D. R. & Wehner, M. F. Is the climate warming or cooling? *Geophys Res Lett* **36**, L08706 (2009).
5. England, M. H. *et al.* Recent intensification of wind-driven circulation in the Pacific and the ongoing warming hiatus. *Nat Clim Chang* **4**, 222–227 (2014).
6. Meehl, G. A., Arblaster, J. M., Fasullo, J. T., Hu, A. & Trenberth, K. E. Model-based evidence of deep-ocean heat uptake during surface-temperature hiatus periods. *Nat Clim Chang* **1**, 360–364 (2011).
7. Cheng, L., Abraham, J., Hausfather, Z. & Trenberth, K. E. How fast are the oceans warming? *Science (1979)* **363**, 128–129 (2019).
8. Cheng, L. *et al.* Past and future ocean warming. *Nat Rev Earth Environ* (2022) doi:10.1038/s43017-022-00345-1.
9. Held, I. M. *et al.* Probing the fast and slow components of global warming by returning abruptly to preindustrial forcing. *J Clim* **23**, 2418–2427 (2010).
10. Solomon, S., Plattner, G.-K., Knutti, R. & Friedlingstein, P. *Irreversible climate change due to carbon dioxide emissions*. www.pnas.org/cgi/content/full/ (2009).
11. Frölicher, T. L., Winton, M. & Sarmiento, J. L. Continued global warming after CO2 emissions stoppage. *Nat Clim Chang* **4**, 40–44 (2014).
12. Hoegh-Guldberg, O., Jacob, D. & Taylor, M. Impacts of 1.5°C of Global Warming on Natural and Human Systems. *Special Report, Intergovernmental Panel on Climate Change* 175–181 (2018).
13. Luderer, G. *et al.* Residual fossil CO2 emissions in 1.5–2 °C pathways. *Nat Clim Chang* **8**, 626–633 (2018).
14. Tong, D. *et al.* Committed emissions from existing energy infrastructure jeopardize 1.5 °C climate target. *Nature* **572**, 373–377 (2019).
15. Welsby, D., Price, J., Pye, S. & Ekins, P. Unextractable fossil fuels in a 1.5 °C world. *Nature* **597**, 230–234 (2021).
16. Boucher, O. *et al.* Reversibility in an Earth System model in response to CO2 concentration changes. *Environmental Research Letters* **7**, (2012).
17. Garbe, J., Albrecht, T., Levermann, A., Donges, J. F. & Winkelmann, R. The hysteresis of the Antarctic Ice Sheet. *Nature* **585**, 538–544 (2020).
18. Jackson, L. C., Schaller, N., Smith, R. S., Palmer, M. D. & Vellinga, M. Response of the Atlantic meridional overturning circulation to a reversal of greenhouse gas increases. *Clim Dyn* **42**, 3323–3336 (2014).
19. Sgubin, G., Swingedouw, D., Drijfhout, S., Hagemann, S. & Robertson, E. Multimodel analysis on the response of the AMOC under an increase of radiative forcing and its symmetrical reversal. *Clim Dyn* **45**, 1429–1450 (2015).

20. Chadwick, R., Wu, P., Good, P. & Andrews, T. Asymmetries in tropical rainfall and circulation patterns in idealised CO2 removal experiments. *Clim Dyn* **40**, 295–316 (2013).
21. Wu, P., Ridley, J., Pardaens, A., Levine, R. & Lowe, J. The reversibility of CO2 induced climate change. *Clim Dyn* **45**, 745–754 (2015).
22. Bouttes, N., Gregory, J. M. & Lowe, J. A. The reversibility of sea level rise. *J Clim* **26**, 2502–2513 (2013).
23. Ehlert, D. & Zickfeld, K. Irreversible ocean thermal expansion under carbon dioxide removal. *Earth System Dynamics* **9**, 197–210 (2018).
24. Oh, J., An, S., Shin, J. & Kug, J. Centennial Memory of the Arctic Ocean for Future Arctic Climate Recovery in Response to a Carbon Dioxide Removal. *Earths Future* **10**, (2022).
25. An, S. *et al.* Global Cooling Hiatus Driven by an AMOC Overshoot in a Carbon Dioxide Removal Scenario. *Earths Future* **9**, (2021).
26. Song, S.-Y. *et al.* Asymmetrical response of summer rainfall in East Asia to CO2 forcing. *Sci Bull (Beijing)* **67**, 213–222 (2022).
27. Kug, J.-S. *et al.* Hysteresis of the intertropical convergence zone to CO2 forcing. *Nat Clim Chang* **12**, 47–53 (2022).
28. Kim, S.-K. *et al.* Widespread irreversible changes in surface temperature and precipitation in response to CO2 forcing. *Nat Clim Chang* **12**, 834–840 (2022).
29. Pathirana, G. *et al. Increase in convective extreme El Niño events in a CO2 removal scenario*. https://www.science.org (2023).
30. Schwinger, J., Asaadi, A., Steinert, N. J. & Lee, H. Emit now, mitigate later? Earth system reversibility under overshoots of different magnitudes and durations. *Earth System Dynamics* **13**, 1641–1665 (2022).
31. Li, X., Zickfeld, K., Mathesius, S., Kohfeld, K. & Matthews, J. B. R. Irreversibility of Marine Climate Change Impacts Under Carbon Dioxide Removal. *Geophys Res Lett* **47**, (2020).
32. Mathesius, S., Hofmann, M., Caldeira, K. & Schellnhuber, H. J. Long-term response of oceans to CO2 removal from the atmosphere. *Nat Clim Chang* **5**, 1107–1113 (2015).
33. Wu, P., Wood, R., Ridley, J. & Lowe, J. Temporary acceleration of the hydrological cycle in response to a CO2 rampdown. *Geophys Res Lett* **37**, 1–5 (2010).
34. Long, S.-M., Xie, S.-P., Zheng, X.-T. & Liu, Q. Fast and Slow Responses to Global Warming: Sea Surface Temperature and Precipitation Patterns. *J Clim* **27**, 285–299 (2014).
35. Long, S. M. *et al.* Effects of ocean slow response under low warming targets. *J Clim* **33**, 477–496 (2020).
36. Xie, S.-P. *et al.* Global Warming Pattern Formation: Sea Surface Temperature and Rainfall*. *J Clim* **23**, 966–986 (2010).
37. Zhou, S., Huang, P., Xie, S.-P., Huang, G. & Wang, L. Varying contributions of fast and slow responses cause asymmetric tropical rainfall change between CO2 ramp-up and ramp-down. *Sci Bull (Beijing)* **67**, 1702–1711 (2022).
38. Li, G. *et al.* Increasing ocean stratification over the past half-century. *Nat Clim Chang* **10**, 1116–1123 (2020).

39. Morrison, A. K., Waugh, D. W., Hogg, A. M., Jones, D. C. & Abernathey, R. P. Ventilation of the Southern Ocean Pycnocline. (2022) doi:10.1146/annurev-marine-010419.
40. Shi, J.-R., Xie, S.-P. & Talley, L. D. Evolving Relative Importance of the Southern Ocean and North Atlantic in Anthropogenic Ocean Heat Uptake. *J Clim* **31**, 7459–7479 (2018).
41. Liu, W., Lu, J., Xie, S.-P. & Fedorov, A. Southern Ocean Heat Uptake, Redistribution, and Storage in a Warming Climate: The Role of Meridional Overturning Circulation. *J Clim* **31**, 4727–4743 (2018).
42. Huguenin, M. F., Holmes, R. M. & England, M. H. Drivers and distribution of global ocean heat uptake over the last half century. *Nat Commun* **13**, 4921 (2022).
43. An, S.-I. *et al.* General circulation and global heat transport in a quadrupling CO2 pulse experiment. *Sci Rep* **12**, 11569 (2022).
44. Gregory, J. & Webb, M. Tropospheric Adjustment Induces a Cloud Component in CO2 Forcing. *J Clim* **21**, 58–71 (2008).
45. Bourgeois, T., Goris, N., Schwinger, J. & Tjiputra, J. F. Stratification constrains future heat and carbon uptake in the Southern Ocean between 30°S and 55°S. *Nat Commun* **13**, (2022).
46. Bronselaer, B. & Zanna, L. Heat and carbon coupling reveals ocean warming due to circulation changes. *Nature* **584**, 227–233 (2020).
47. Gent, P. R. & Mcwilliams, J. C. Isopycnal mixing in ocean circulation models. *J Phys Oceanogr* **20**, 150–155 (1990).
48. Wu, P., Jackson, L., Pardaens, A. & Schaller, N. Extended warming of the northern high latitudes due to an overshoot of the Atlantic meridional overturning circulation. *Geophys Res Lett* **38**, 1–5 (2011).
49. Redi, M. H. Oceanic isopycnal mixing by coordinate rotation. *J Phys Oceanogr* **12**, 1154–1158 (1982).
50. Stuecker, M. F. *et al.* Polar amplification dominated by local forcing and feedbacks. *Nat Clim Chang* **8**, 1076–1081 (2018).
51. Mechoso, C. R. *et al.* Can reducing the incoming energy flux over the Southern Ocean in a CGCM improve its simulation of tropical climate? *Geophys Res Lett* **43**, 11,057-11,063 (2016).
52. Kim, H., Kang, S. M., Kay, J. E., Xie, S.-P. & Hartmann, D. Subtropical clouds key to Southern Ocean teleconnections to the tropical Pacific. (2022) doi:10.1073/pnas.
53. Schneider, T., Bischoff, T. & Haug, G. H. Migrations and dynamics of the intertropical convergence zone. *Nature* **513**, 45–53 (2014).
54. Bischoff, T. & Schneider, T. Energetic constraints on the position of the intertropical convergence zone. *J Clim* **27**, 4937–4951 (2014).
55. White, R. H. *et al.* Tropical Precipitation and Cross-Equatorial Heat Transport in Response to Localized Heating: Basin and Hemisphere Dependence. *Geophys Res Lett* **45**, 11,949-11,958 (2018).
56. Byrne, M. P., Pendergrass, A. G., Rapp, A. D. & Wodzicki, K. R. Response of the Intertropical Convergence Zone to Climate Change: Location, Width, and Strength. *Curr Clim Change Rep* **4**, 355–370 (2018).

57. Cai, W. *et al.* Increasing frequency of extreme El Niño events due to greenhouse warming. *Nat Clim Chang* **4**, 111–116 (2014).
58. Hoskins, B. J. & Karoly, D. J. The Steady Linear Response of a Spherical Atmosphere to Thermal and Orographic Forcing. *J Atmos Sci* **38**, 1179–1196 (1981).
59. Goosse, H. *et al.* Quantifying climate feedbacks in polar regions. *Nat Commun* **9**, 1919 (2018).

**Methods-only references**


60 Keller, D. P. *et al.* The Carbon Dioxide Removal Model Intercomparison Project (CDRMIP): Rationale and experimental protocol for CMIP6. *Geosci Model Dev* **11**, 1133–1160 (2018).

61 Oh, J.-H. Data and codes for "Emergent climate change patterns originating from deep ocean warming in climate mitigation scenarios". https://doi.org/10.6084/m9.figshare.24873216.v1 (2023).

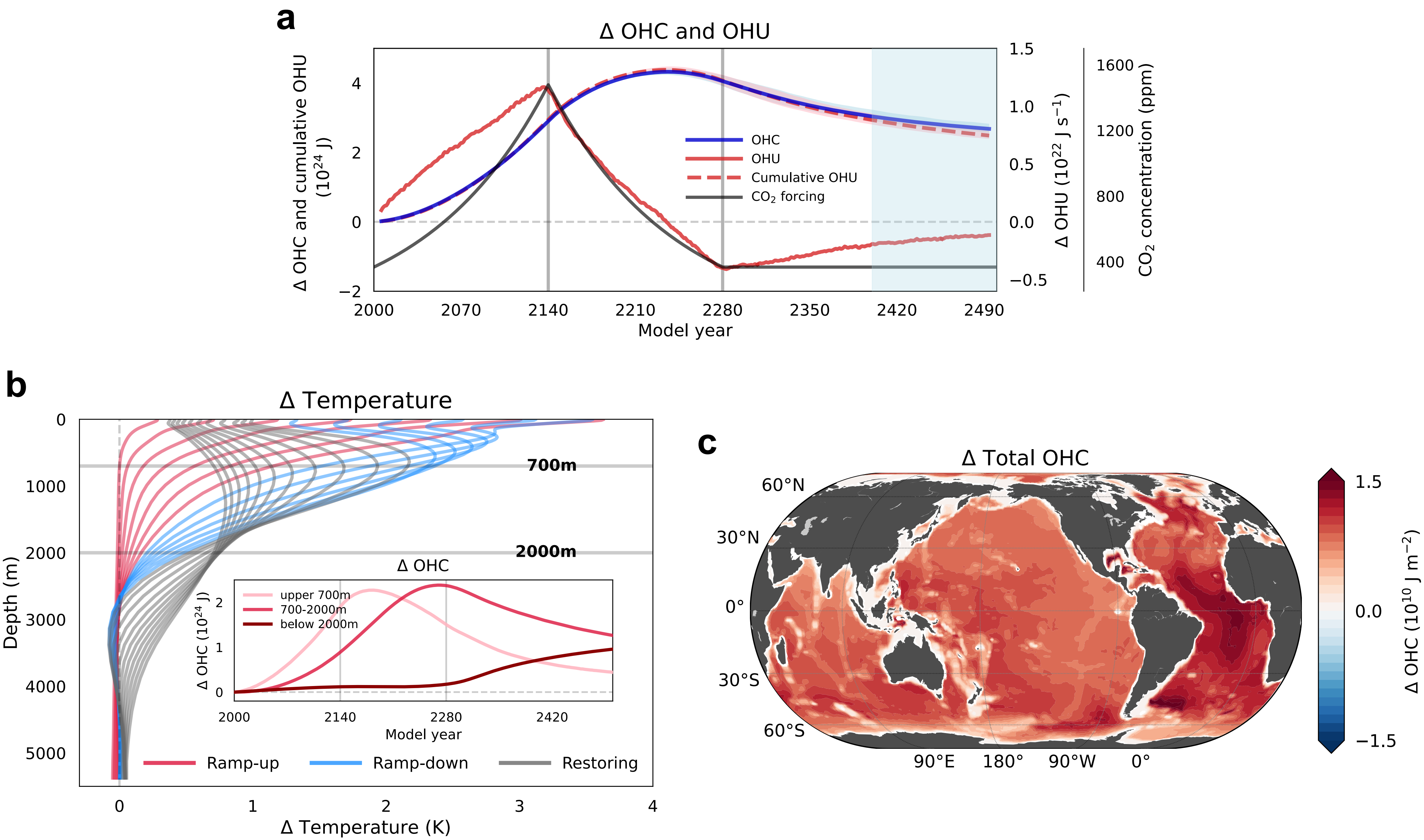

a
Δ OHC and OHU
Δ OHC and cumulative OHU (10^24 J)
Δ OHU (10^22 J s^−1)
CO2 concentration (ppm)
OHC
OHU
Cumulative OHU
CO2 forcing
Model year
b
Δ Temperature
700m
2000m
Depth (m)
Δ OHC
upper 700m
700-2000m
below 2000m
Δ OHC (10^24 J)
Model year
Ramp-up
Ramp-down
Restoring
Δ Temperature (K)
c
Δ Total OHC
60°N
30°N
0°
30°S
60°S
90°E
180°
90°W
0°
Δ OHC (10^10 J m^−2)

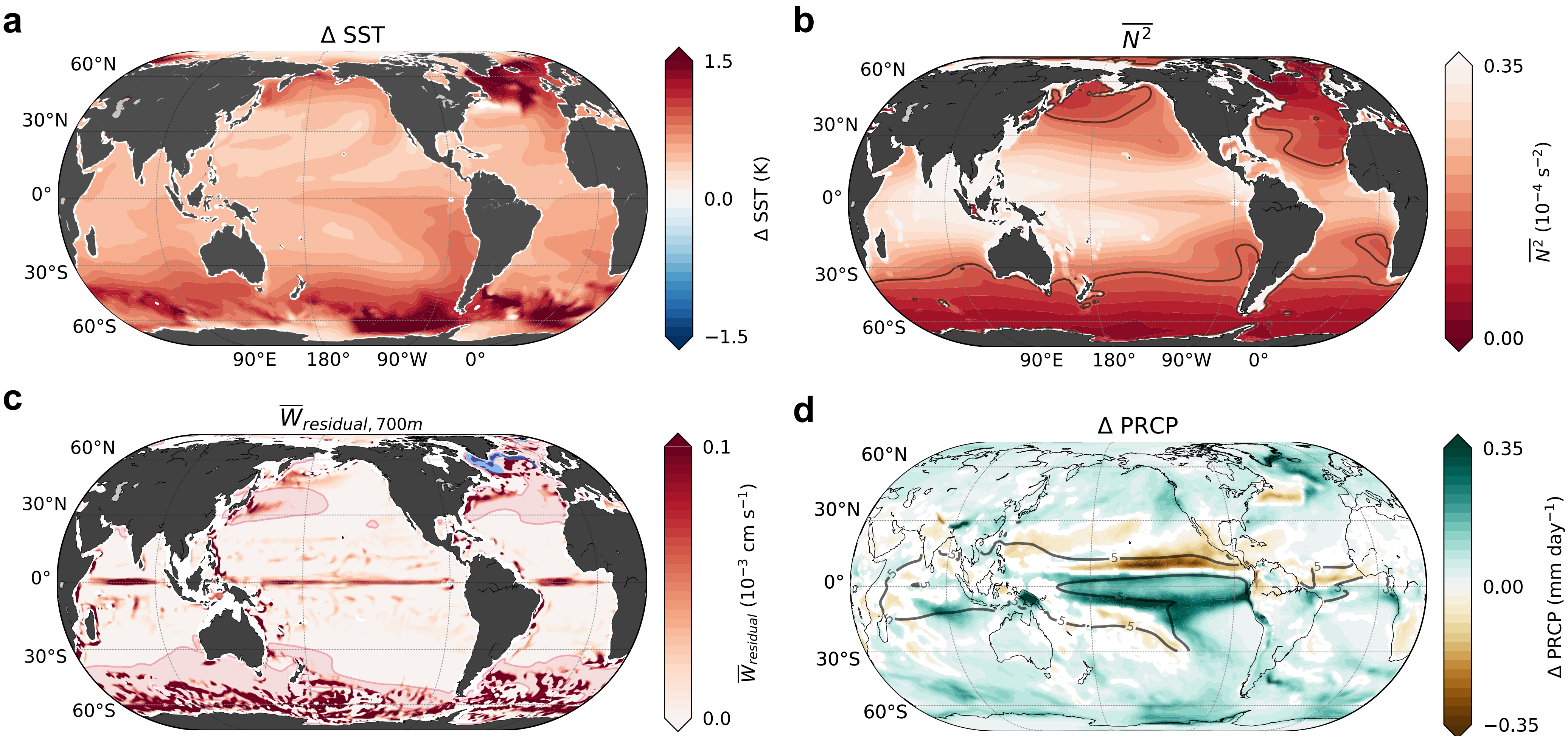

a
Δ SST
60°N
30°N
0°
30°S
60°S
90°E
180°
90°W
0°
1.5
0.0
−1.5
Δ SST (K)
b
$\overline{N^2}$
0.35
0.00
$\overline{N^2}$ ($10^{-4}$ s$^{-2}$)
c
$\overline{W}_{residual, 700m}$
0.1
0.0
$\overline{W}_{residual}$ ($10^{-3}$ cm s$^{-1}$)
d
Δ PRCP
5
0.35
0.00
−0.35
Δ PRCP (mm day$^{-1}$)

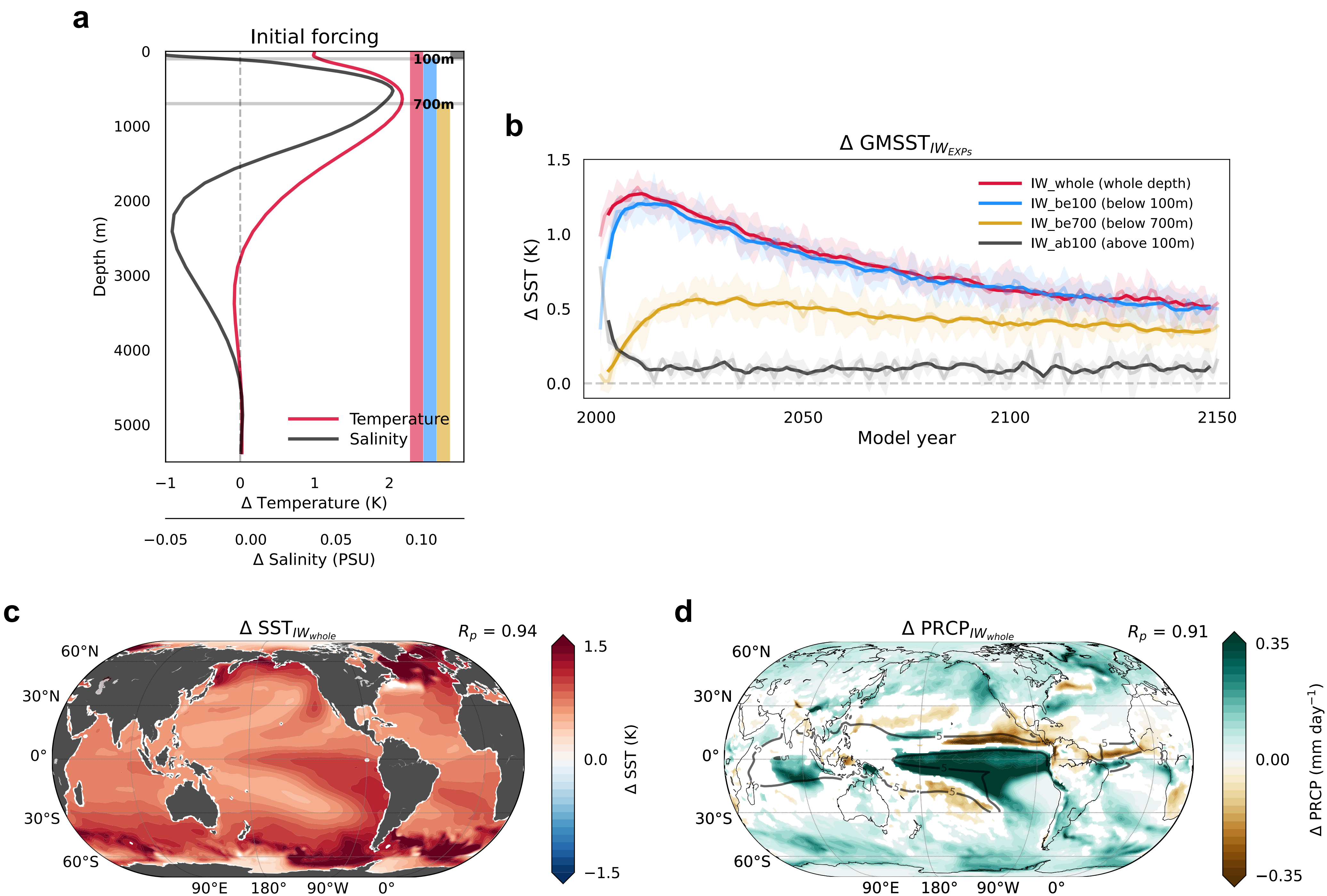

a
Initial forcing
100m
700m
Depth (m)
Temperature
Salinity
Δ Temperature (K)
Δ Salinity (PSU)
b
Δ GMSST$_{IW_{EXPs}}$
IW_whole (whole depth)
IW_be100 (below 100m)
IW_be700 (below 700m)
IW_ab100 (above 100m)
Δ SST (K)
Model year
c
Δ SST$_{IW_{whole}}$
$R_p$ = 0.94
Δ SST (K)
d
Δ PRCP$_{IW_{whole}}$
$R_p$ = 0.91
Δ PRCP (mm day$^{-1}$)

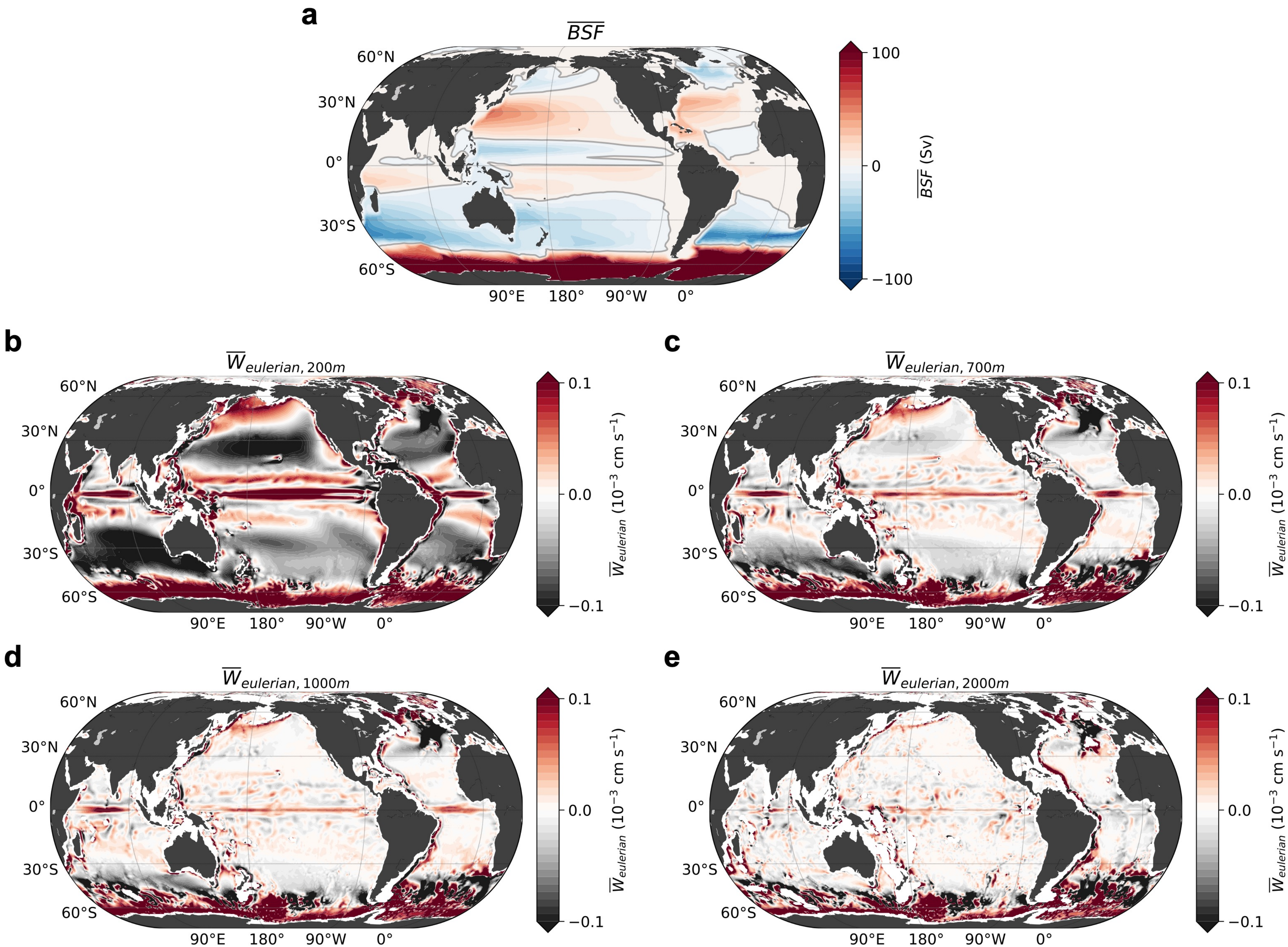

a
$\overline{BSF}$
60°N
30°N
0°
30°S
60°S
90°E
180°
90°W
0°
100
0
−100
$\overline{BSF}$ (Sv)
b
$\overline{W}_{eulerian,200m}$
c
$\overline{W}_{eulerian,700m}$
d
$\overline{W}_{eulerian,1000m}$
e
$\overline{W}_{eulerian,2000m}$
0.1
0.0
−0.1
$\overline{W}_{eulerian}$ ($10^{-3}$ cm s$^{-1}$)

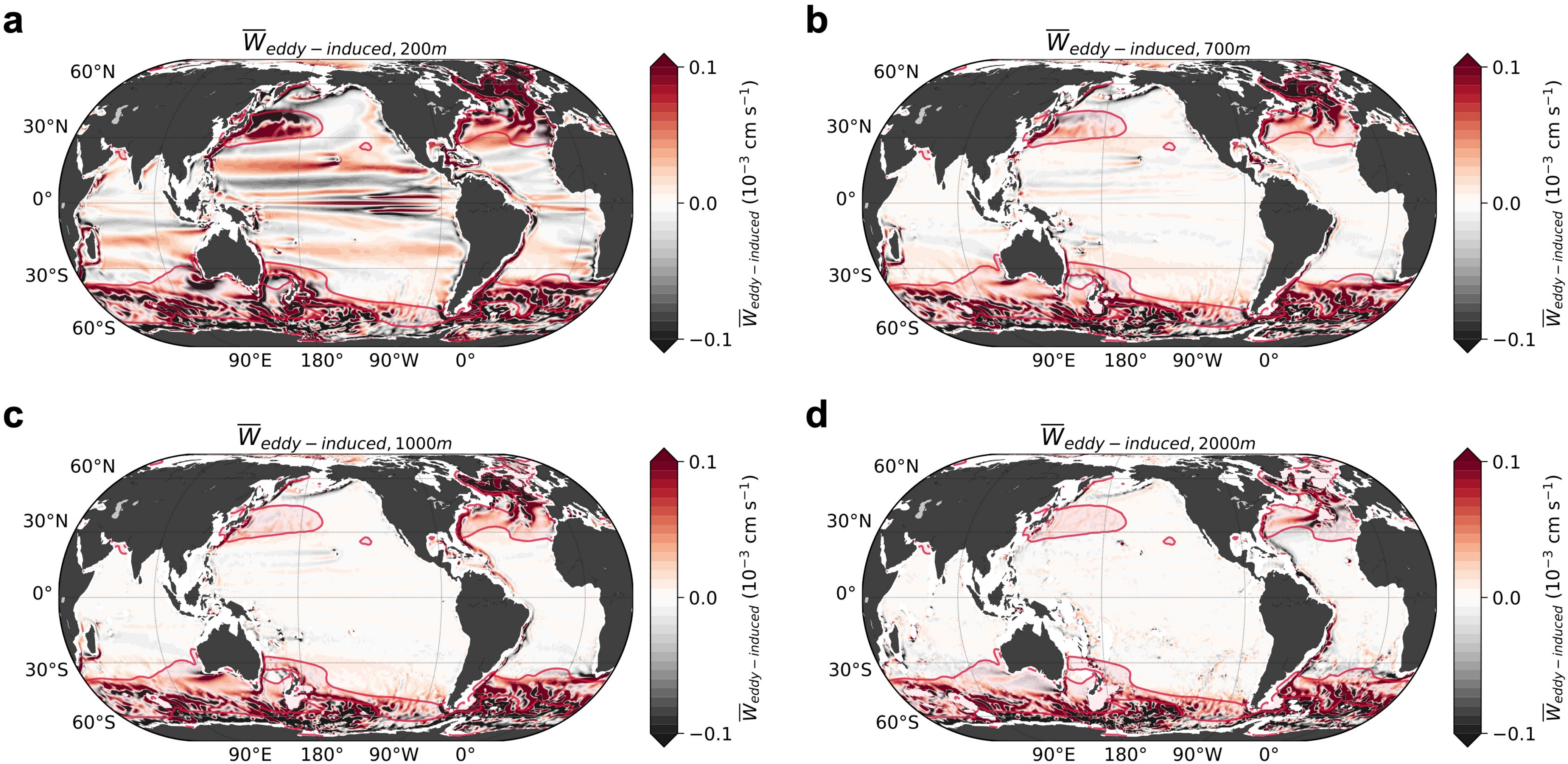

a
$\overline{W}_{eddy-induced, 200m}$
b
$\overline{W}_{eddy-induced, 700m}$
c
$\overline{W}_{eddy-induced, 1000m}$
d
$\overline{W}_{eddy-induced, 2000m}$
60°N
30°N
0°
30°S
60°S
90°E
180°
90°W
0°
0.1
0.0
−0.1
$\overline{W}_{eddy-induced}$ ($10^{-3}$ cm s$^{-1}$)

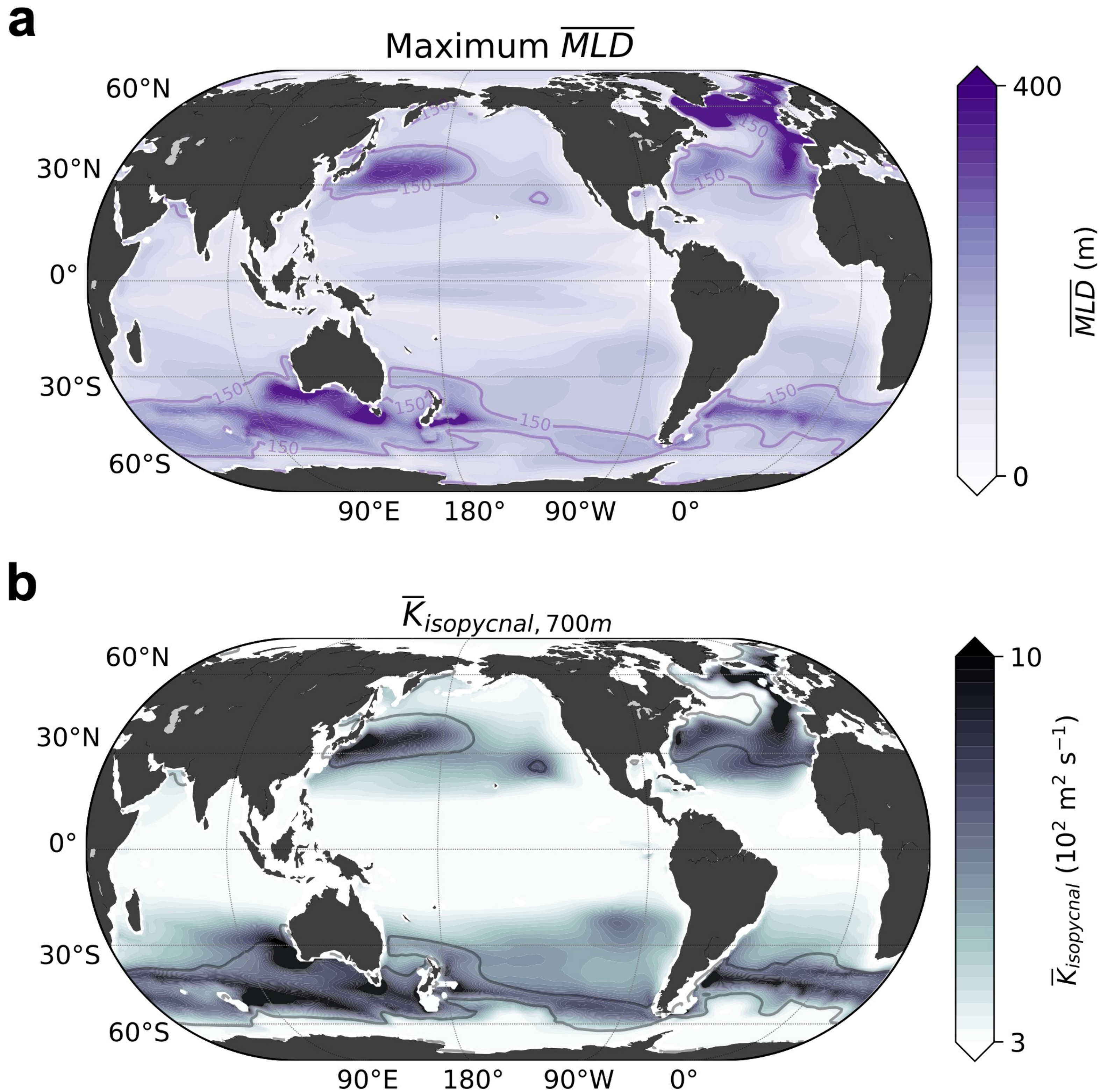
a
Maximum $\overline{MLD}$
60°N
30°N
0°
30°S
60°S
90°E
180°
90°W
0°
150
400
0
$\overline{MLD}$ (m)
b
$\overline{K}_{isopycnal,700m}$
60°N
30°N
0°
30°S
60°S
90°E
180°
90°W
0°
10
3
$\overline{K}_{isopycnal}$ ($10^2$ m$^2$ s$^{-1}$)

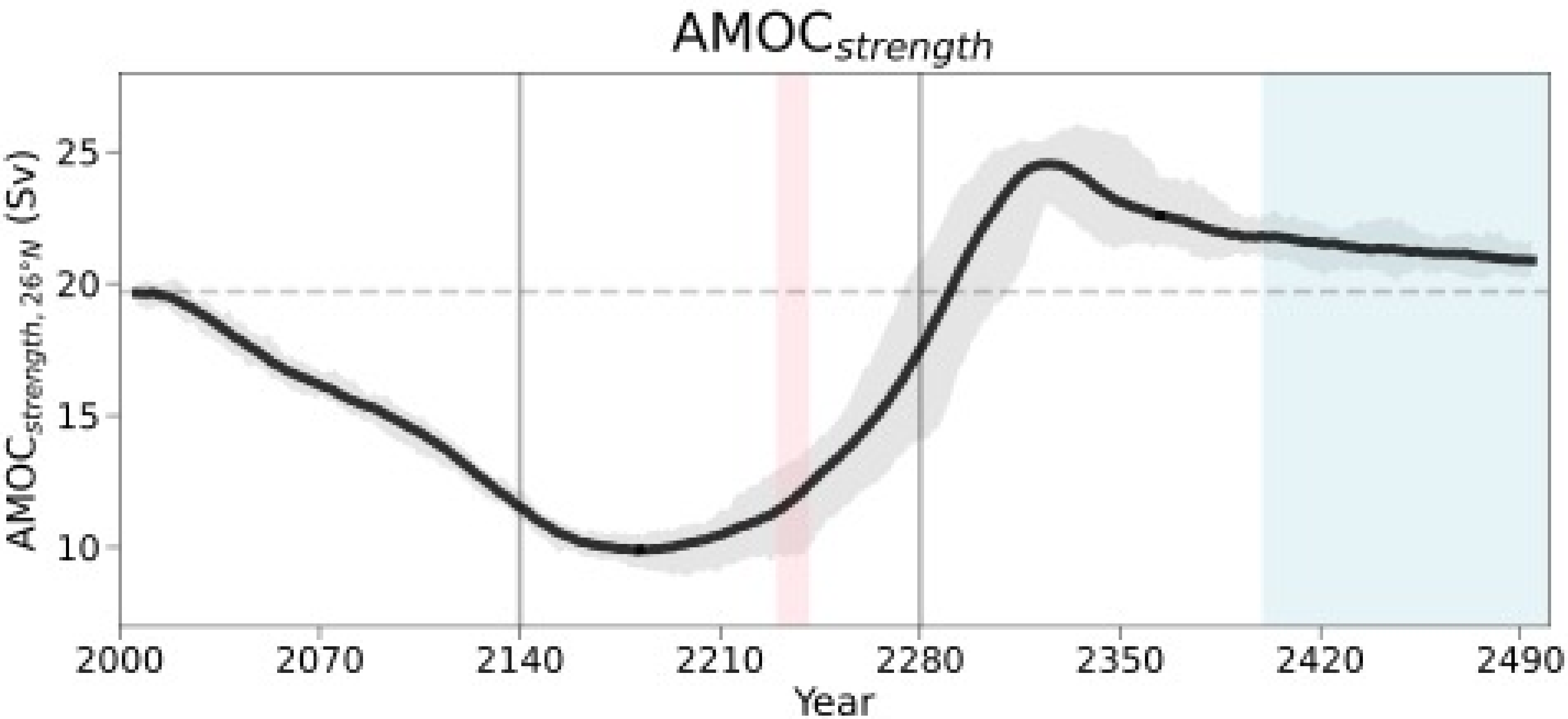

AMOC$_{strength}$
AMOC$_{strength,\ 26°N}$ (Sv)
25
20
15
10
2000
2070
2140
2210
2280
2350
2420
2490
Year

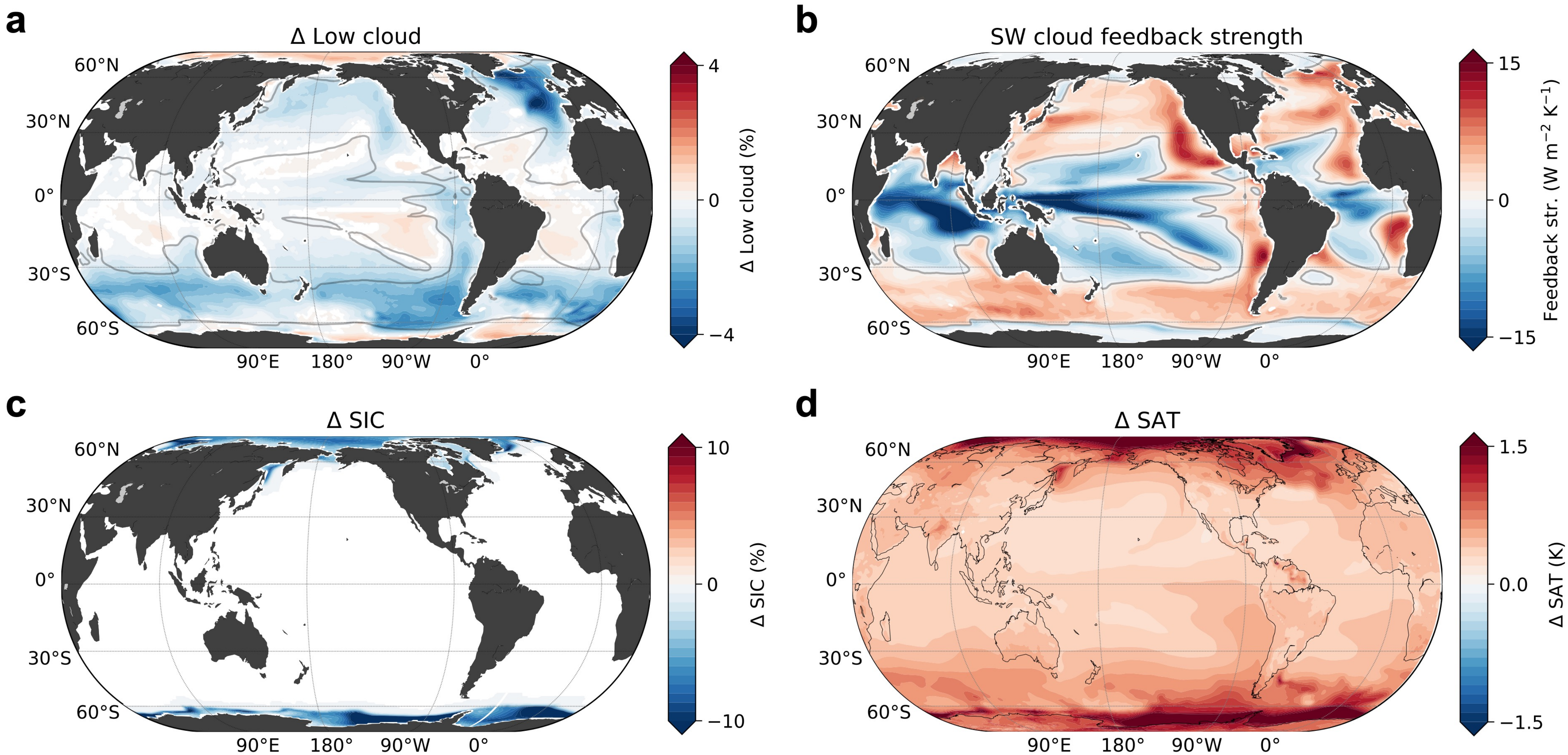

a
Δ Low cloud
Δ Low cloud (%)
4
0
−4
b
SW cloud feedback strength
Feedback str. (W m$^{-2}$ K$^{-1}$)
15
0
−15
c
Δ SIC
Δ SIC (%)
10
0
−10
d
Δ SAT
Δ SAT (K)
1.5
0.0
−1.5
60°N
30°N
0°
30°S
60°S
90°E
180°
90°W
0°

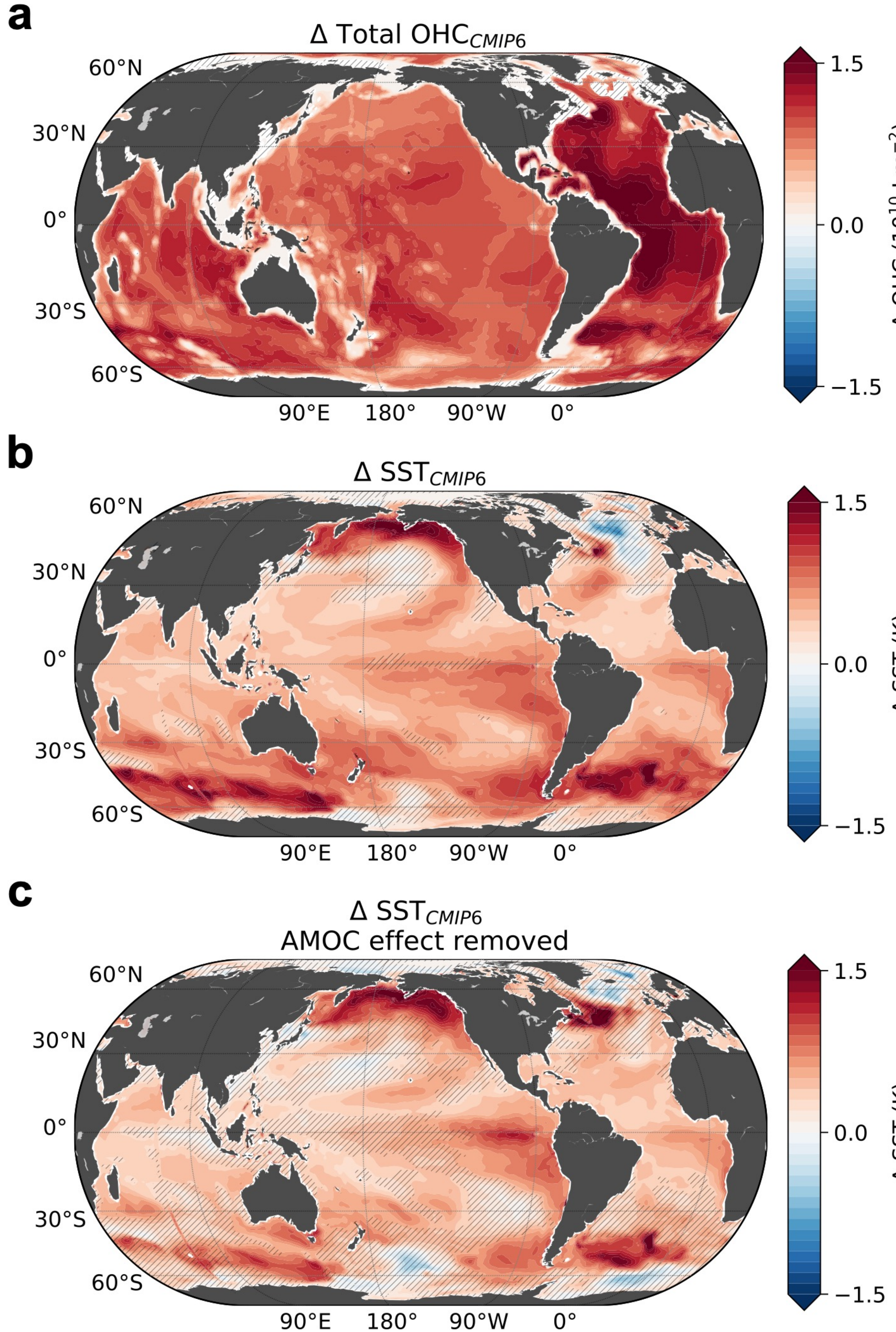
a
Δ Total OHC$_{CMIP6}$
60°N
30°N
0°
30°S
60°S
90°E
180°
90°W
0°
1.5
0.0
−1.5
Δ OHC ($10^{10}$ J m$^{-2}$)
b
Δ SST$_{CMIP6}$
60°N
30°N
0°
30°S
60°S
90°E
180°
90°W
0°
1.5
0.0
−1.5
Δ SST (K)
c
Δ SST$_{CMIP6}$
AMOC effect removed
60°N
30°N
0°
30°S
60°S
90°E
180°
90°W
0°
1.5
0.0
−1.5
Δ SST (K)

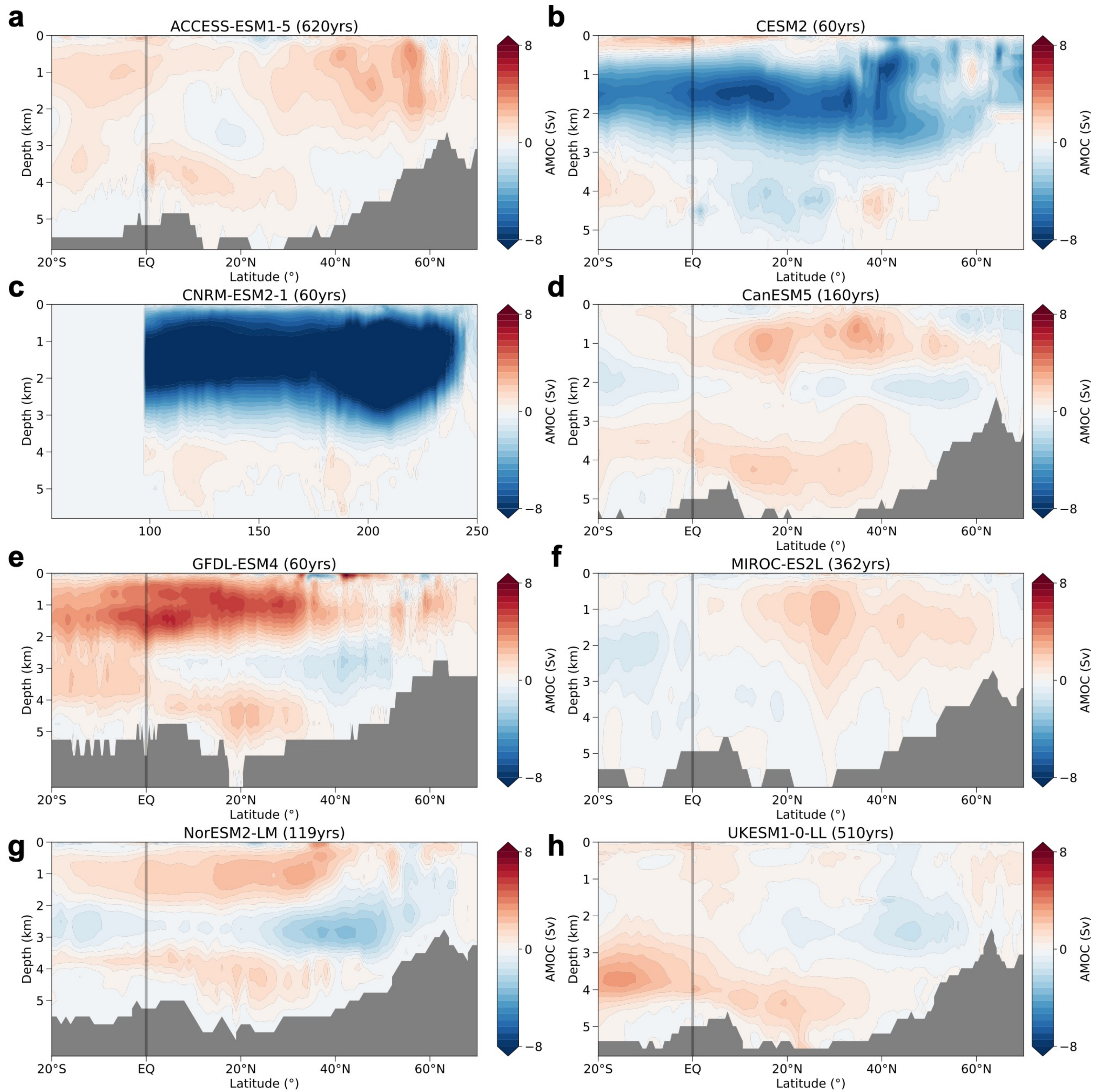

a
ACCESS-ESM1-5 (620yrs)
b
CESM2 (60yrs)
c
CNRM-ESM2-1 (60yrs)
d
CanESM5 (160yrs)
e
GFDL-ESM4 (60yrs)
f
MIROC-ES2L (362yrs)
g
NorESM2-LM (119yrs)
h
UKESM1-0-LL (510yrs)
Depth (km)
Latitude (°)
AMOC (Sv)
20°S
EQ
20°N
40°N
60°N
100
150
200
250
8
0
−8

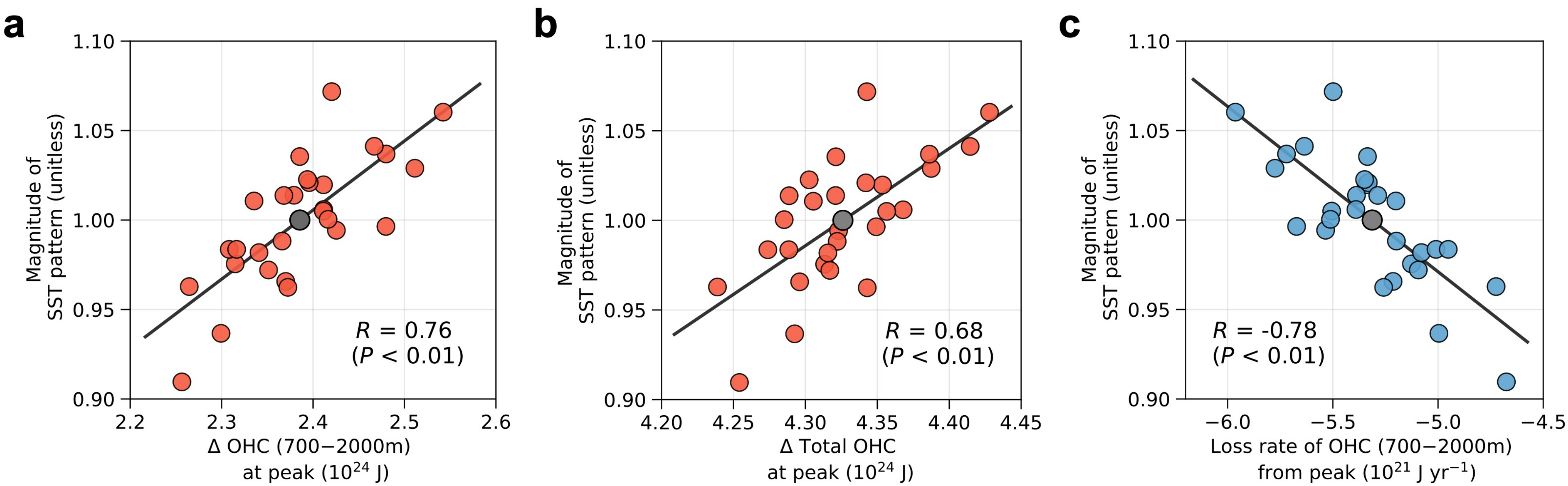
a
b
c
Magnitude of SST pattern (unitless)
R = 0.76 (P < 0.01)
Δ OHC (700−2000m) at peak (10^24 J)
R = 0.68 (P < 0.01)
Δ Total OHC at peak (10^24 J)
R = -0.78 (P < 0.01)
Loss rate of OHC (700−2000m) from peak (10^21 J yr^−1)

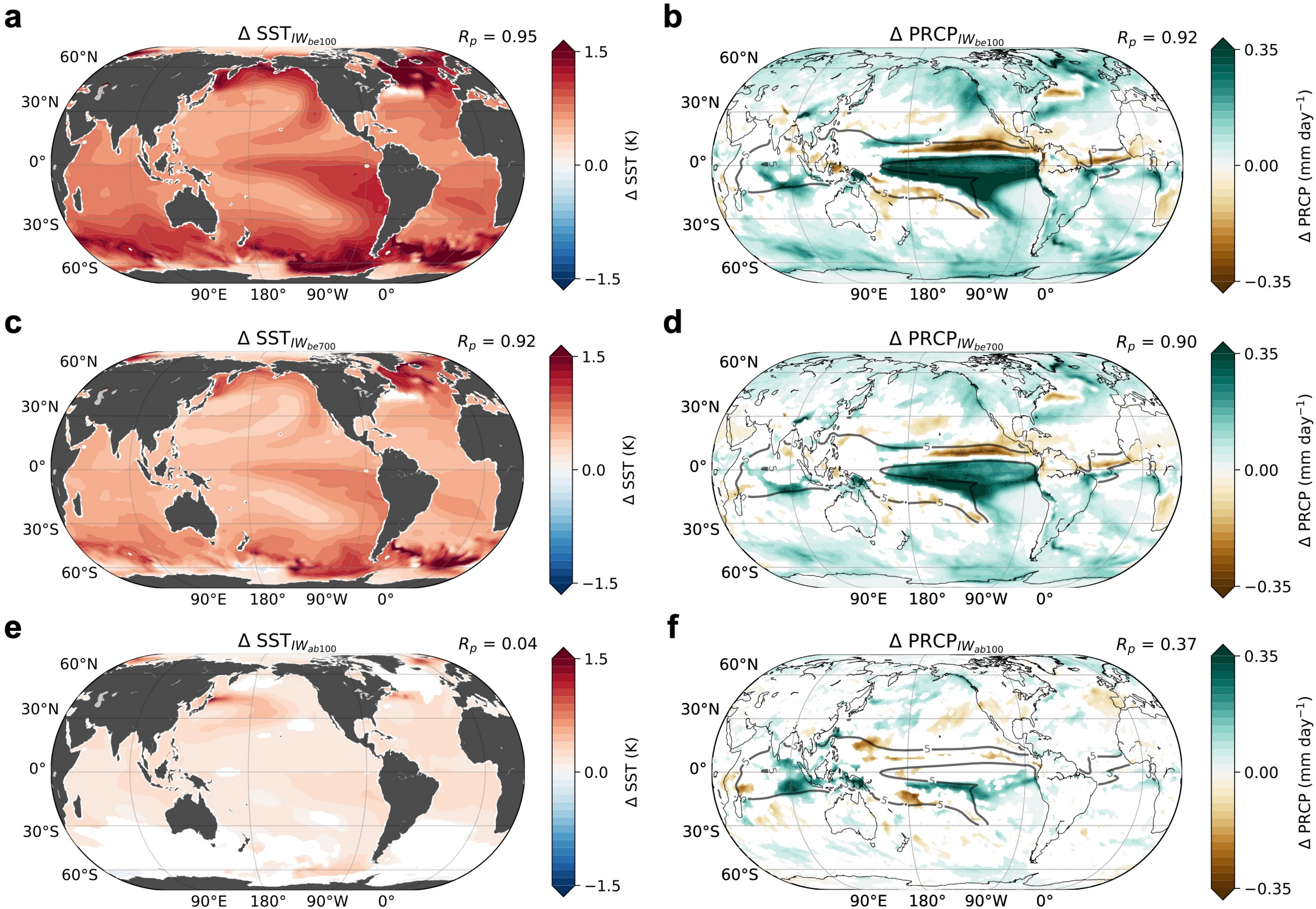

a
Δ SST$_{IW_{be100}}$
$R_p$ = 0.95
b
Δ PRCP$_{IW_{be100}}$
$R_p$ = 0.92
c
Δ SST$_{IW_{be700}}$
$R_p$ = 0.92
d
Δ PRCP$_{IW_{be700}}$
$R_p$ = 0.90
e
Δ SST$_{IW_{ab100}}$
$R_p$ = 0.04
f
Δ PRCP$_{IW_{ab100}}$
$R_p$ = 0.37
60°N
30°N
0°
30°S
60°S
90°E
180°
90°W
0°
1.5
0.0
−1.5
Δ SST (K)
0.35
0.00
−0.35
Δ PRCP (mm day$^{-1}$)
5

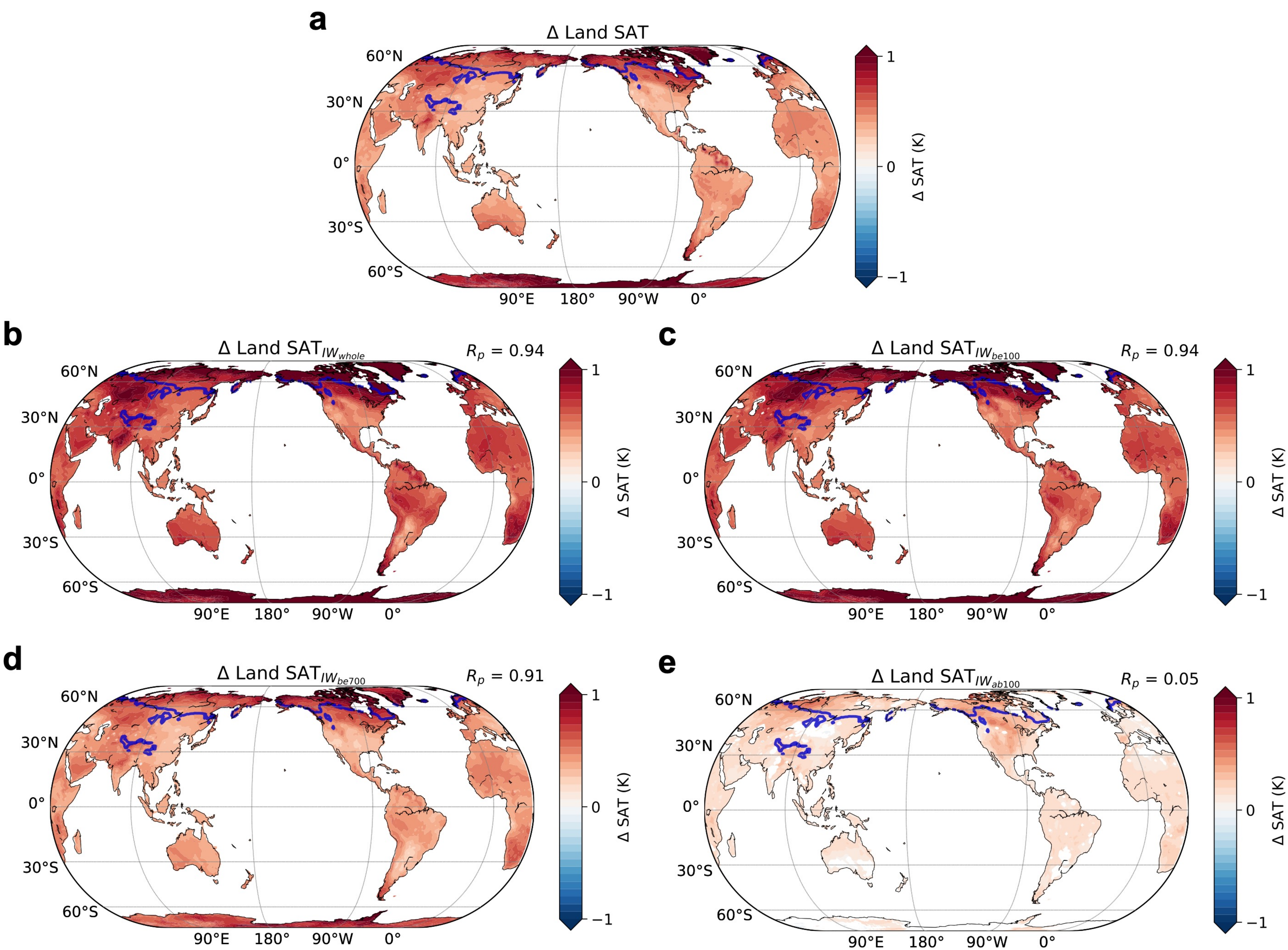

a
Δ Land SAT
b
Δ Land SAT$_{IW_{whole}}$
$R_p$ = 0.94
c
Δ Land SAT$_{IW_{be100}}$
$R_p$ = 0.94
d
Δ Land SAT$_{IW_{be700}}$
$R_p$ = 0.91
e
Δ Land SAT$_{IW_{ab100}}$
$R_p$ = 0.05
60°N
30°N
0°
30°S
60°S
90°E
180°
90°W
0°
Δ SAT (K)
1
0
−1